Published in final edited form as:
Circ Cardiovasc Imaging. 2014 July ; 7(4): 697–705. doi:10.1161/CIRCIMAGING.113.001806.

In Vivo Molecular Imaging of Thrombosis and Thrombolysis Using a Fibrin-binding Positron Emission Tomography Probe

Ilknur Ay, MD, PhD, **Francesco Blasi, PharmD, PhD**, **Tyson A. Rietz, BS**, **Nicholas J. Rotile, BA**, **Sreekanth Kura, MS**, **Anna Liisa Brownell, PhD**, **Helen Day, MS**, **Bruno L. Oliveira, PhD**, **Richard J. Looby, BS**, and **Peter Caravan, PhD**
Athinoula A. Martinos Center for Biomedical Imaging, Department of Radiology, Massachusetts General Hospital, Charlestown, MA

Abstract

Background—Fibrin is a major component of arterial and venous thrombi and represents an ideal candidate for molecular imaging of thrombosis. Here, we describe imaging properties and target uptake of a new fibrin-specific PET probe for thrombus detection and therapy monitoring in two rat thrombosis models.

Methods and Results—The fibrin-binding probe FBP7 was synthesized by conjugation of a known short cyclic peptide to a cross-bridged chelator (CB-TE2A), followed by labeling with copper-64. Adult male Wistar rats (n=26) underwent either carotid crush injury (mural thrombosis model) or embolic stroke (occlusive thrombosis model) followed by rtPA treatment (10 mg/kg, i.v.). FBP7 detected thrombus location in both animal models with a high PET target-to-background ratio that increased over time (>5-fold at 30–90 min, >15-fold at 240–285 min). In the carotid crush injury animals, biodistribution analysis confirmed high probe uptake in the thrombotic artery (~0.5 %ID/g; >5-fold greater than blood and other tissues of the head and thorax). Similar results were obtained from ex vivo autoradiography of the ipsilateral vs. contralateral carotid arteries. In embolic stroke animals, PET-CT imaging localized the clot in the internal carotid/middle cerebral artery segment of all rats. Time-dependent reduction of activity at the level of the thrombus was detected in rtPA-treated rats but not in vehicle-injected animals. Brain autoradiography confirmed clot dissolution in rtPA-treated animals, but enduring high thrombus activity in control rats.

Conclusions—We demonstrated that FBP7 is suitable for molecular imaging of thrombosis and thrombolysis in vivo, and represents a very promising candidate for bench-to-bedside translation.

Keywords

thrombosis; PET imaging; fibrin; thrombolysis; stroke

Correspondence to: Peter Caravan, PhD, Building 149, Room 2301, 13th Street, Charlestown, MA 02129, Phone: 617-643-0193, Fax: 617-726-7422, caravan@nmr.mgh.harvard.edu.
Drs. Ay and Blasi contributed equally to this work.

Disclosures
Peter Caravan has equity in Factor 1A, LLC, the company holding the patent rights to the peptide used in this work. The other authors report no conflicts.

Thrombosis, the underlying cause in the majority of cardiovascular disorders, has a high incidence and prevalence in the US[1]. Recent advances in medical imaging have facilitated the diagnosis of thrombotic and thromboembolic disorders; however some challenges still remain. First, although recurrences occur in most cases, diagnostic techniques including magnetic resonance (MR) imaging and computed tomography (CT) are not very efficient to identify the source thrombus, especially when used as a single test.[2, 3] Identification of source thrombus requires a technique with whole body scanning and high sensitivity. Second, modalities that are used to detect thrombus, including carotid or pelvic ultrasound, transesophageal echocardiogram (TEE), CT, and MRI have some pitfalls with respect to sensitivity, specificity, and feasibility.[4–7] Multimodal imaging with a molecular probe designed to detect thrombus offers a potential solution to both of these challenges.[8, 9] So far, coagulation factors (thrombin, Factor XIII, fibrinogen, fibrin) and activated platelets have been targeted for molecular thrombus imaging.[10] Among them, fibrin represents an ideal target due to its high specificity (present at high concentration in all clots but not in circulating blood) and high sensitivity (present in all thrombi whether arterial or venous, fresh or aged).[11]

PET is a quantitative, high sensitivity technique that offers the possibility for whole body scanning. Hybrid imaging that combines PET with CT, or more recently PET with MR, provides a high resolution anatomical image (CT or MR) onto which the lower resolution molecular PET image can be overlaid. Thus a sensitive thrombus-specific PET probe may detect even minor thrombotic events and CT or MR can localize this PET activity to a specific location in the vascular tree. An ideal fibrin/thrombus PET probe should have high affinity for fibrin, high specificity for fibrin over fibrinogen and other blood proteins, rapid clearance from the circulation to increase thrombus-to-background ratio, and small size to enable penetration into thrombi. To this end we have labeled a short cyclic peptide that was previously shown to exhibit high affinity for fibrin and great specificity for fibrin versus fibrinogen (>100-fold) and other serum proteins.[12–14] We recently demonstrated preliminary efficacy of PET and bimodal PET-MR probes based on these fibrin-specific binding peptides for molecular imaging of thrombus, although these probes suffered from instability *in vivo*.[15–17] In the present study, we report the efficacy of a newly developed, chemically stable, fibrin-binding PET probe termed FBP7 in two different animal models of arterial thrombosis: carotid crush injury as a non-occlusive intramural thrombosis model and embolic stroke as an occlusive thrombosis model. To extend the translational outcome of our work, we also tested whether FBP7 was able to visualize and quantify *in vivo* thrombolysis after recombinant tissue plasminogen activator (rtPA) treatment in embolic stroke.

Methods

Synthesis and characterization of FBP7

FBP7 was synthesized by conjugation of the CB-TE2A chelator to a cyclic, disulfide bridged 11-amino acid fibrin-binding peptide, followed by labeling with copper-64 and HPLC purification.[16] The cyclic peptide was previously shown to be effective for fibrin targeting.[14, 16] FBP7 was evaluated for *in vitro* fibrin affinity in the presence and absence of

heparin and also for its plasma stability. Additional information regarding reagents and methods are reported in Supplemental Material.

Animal thrombosis models

All animal experiments were performed in accordance with the NIH Guide for the Care and Use of Laboratory Animals and were approved by the Institutional Animal Care and Use Committee at Massachusetts General Hospital. Adult male Wistar rats (330–400 g; Charles River Laboratories) were anesthetized by isoflurane (4% for induction, 2–2.5% for maintenance in medical air) and were kept under anesthesia throughout the study. Body temperature was maintained at 37–38°C using a thermo-regulated heating pad (Harvard Apparatus). The right femoral vein and artery were catheterized using PE-50 tubing for probe/drug injection and blood sampling, respectively.

Intramural thrombus was induced by carotid artery crush injury (n=10). Under isoflurane anesthesia, the right common carotid artery was exposed and crush injury was induced by clamping the vessel with a hemostat for 5 min, as previously described.[16] Injury was performed 1–2 cm proximal to the carotid bifurcation, using the same hemostat and by the same investigator to minimize variability.

Occlusive thrombus was produced by embolic stroke (n=16) using a previously published method.[18] Briefly, homologous thrombus was prepared one day before by retaining freshly collected arterial blood in a PE50 tube for 2 hours at room temperature and 22 hours at 4°C. The next day, a single 25-mm long clot was injected into the right internal carotid artery (ICA) via an external carotid stump to occlude the middle cerebral artery (MCA) under isoflurane anesthesia. In a subgroup of animals the clot was incubated in an Evans blue solution (2%, w/v) to enhance post-mortem clot visualization.[19] Approximately 1 hour after the clot injection, rats were injected with either rtPA (alteplase, 10 mg/kg, i.v., 10% bolus and 90% infusion over 30 min; n=9) or vehicle (saline solution, 1 mL; n=7). Since the embolic stroke model is associated with a small but significant mortality and failure rate, rats that died during the study period, had hemorrhage at the base of the skull, and were unresponsive to rtPA-induced thrombolysis were considered technical failures and excluded from the final analysis.

PET-CT Imaging

Immediately after the surgical procedures, animals were placed in a dedicated small-animal PET/SPECT/CT scanner (Triumph; TriFoil Imaging), equipped with inhalation anesthesia and heating pad system. Instrument calibration was performed with phantoms containing small known amounts of radioactivity.

FBP7 PET probe was injected 15–30 min after the end of the surgical procedures. Each rat was injected with ~300 μCi probe solution in 0.3–0.4 mL, followed by saline flush. The total activity injected was calculated by subtracting the activity in the syringe before injection from the activity remaining in the syringe after injection as measured by a dose calibrator (Capintec CRC-25PET).

A CT scan with contrast (iopamidol, Isovue 370, Bracco; 0.3 mL/min, i.v.) was performed either before or at the end of the PET acquisition. Isotropic (0.3 mm) CT images were acquired over 6 min with 512 projections with 3 frames per projection (exposure time per frame, ~200 msec; peak tube voltage, 70 kV; tube current, 177 mA). PET and CT images were reconstructed using the LabPET software (TriFoil Imaging) and the CT data were used to provide attenuation correction for the PET reconstructions. The PET data were reconstructed using a maximum-likelihood expectation-maximization (MLEM) algorithm run over 30 iterations to a voxel size of $0.5\times0.5\times0.6$ mm^3. For the pharmacokinetic analyses, the PET data were reconstructed in 1 min (first 10 frames), 3 min (next 10 frames), and 10 min (last 5 frames) intervals out to 90 min post injection. For the embolic stroke experiments, the PET data were reconstructed in 10 min intervals.

Imaging protocols are described in Figure 1. In crush experiments, rats were imaged for 90 min immediately after the injection of the FBP7 or for 45 min at 4 hours post-injection (p.i.). In stroke experiments, animals were imaged for 45 min to acquire a baseline image and then for 90 min starting at the same time of rtPA or vehicle administration.

All animals were euthanized at the end of the imaging session; tissues were harvested and processed for *ex vivo* analyses.

Biodistribution, blood analyses, and autoradiography

To quantify the blood clearance and body distribution of FBP7, radioactivity in the arterial blood samples (collected at 0, 2, 5, 10, 15, 30, 60, 120, 240, and 300 min p.i.) as well as tissues obtained after euthanasia were measured.[16] Blood samples and urine were analyzed by radio-HPLC to evaluate the metabolic stability of FBP7.[16] We also measured the fraction of activity in each plasma sample that was capable of binding to fibrin immobilized on a well plate, and compared this to pure probe spiked into plasma as a means of assaying for functional probe.[16] The right and left common carotid arteries from crush experiments and the brain sections (2 mm-thick, coronal or horizontal) from stroke experiments were analyzed by autoradiography.[16] Additional information is reported in Supplemental Material.

Data Analysis

Reconstructed PET-CT data were quantitatively evaluated using PMOD 3.2 (PMOD Technologies Ltd, Zurich, Switzerland) and AMIDE software packages.[20] For the MCA occlusion model, volumes of interest (VOI) in the right and left MCA (0.8 mm^3) and extracranial ICA (6.3 mm^3) were drawn based on CT landmarks. For the crush injury model, the fused, co-registered CT and PET images were used to localize the hot spot at the site of the injured common carotid artery and a 12.5 mm^3 VOI was placed at this hot spot and at the same level in the contralateral vessel. Brain, heart, and contralateral arterial regions were used to measure background signal. Results were expressed as percent injected dose per cubic centimeter of tissue (%ID/cc).

Autoradiography data were quantified using PerkinElmer OptiQuant 5.0 software. Regions of interest (ROI) were drawn around the ipsilateral (injured) and contralateral carotid

arteries for crush experiments and ipsilateral and contralateral ICA/MCA segments for stroke experiments. Ipsi:contra activity ratios were obtained by dividing matched ipsilateral and contralateral raw values from each animal.

Data were expressed as mean ± SEM. Differences between groups were compared using Student's t-test and ANOVA (one-way or repeated measures) followed by Dunnett's or Bonferroni's post hoc test, whenever appropriate. A P value <0.05 was considered significant.

Results

Probe synthesis and fibrin affinity assay

FBP7 was obtained by reaction of the ligand with $^{64}CuCl_2$ and gave radiochemical purity ≥97% (Supplemental Figure I). FBP7 was highly stable when incubated in rat plasma for up to 16 hours at 37°C.

FBP7 had nanomolar affinity (660 nM) for the soluble fibrin fragment DD(E) and this affinity was not altered by the presence of heparin (5U/ml, Supplemental Figure II).

Pharmacokinetics and metabolism

Analysis of blood samples taken over a 2 hour period showed rapid clearance of the probe with a terminal blood half-life of 18.1±11.9 min (Supplemental Figure IIIA). Blood plasma at each time point was also incubated with fibrin immobilized in a well plate and the fraction of activity bound to fibrin was compared to the result obtained for pure FBP7 spiked into plasma. This functional assay confirmed that >90% of the probe was intact at 1 hour post-injection. HPLC analysis of plasma and urine showed very little degradation of the probe, with ≥75% of the circulating dose existing as intact probe in the plasma at all time points tested (Supplemental Figure IIIB), and just few metabolites in urine and plasma at 2 and 4 hours p.i., respectively (Supplemental Figure IIIC).

Carotid crush injury

The fibrin-binding PET probe FBP7 detected the carotid arterial thrombus in all of the crush injury animals. Representative CT, PET and PET-CT sagittal views are shown in Figure 2. The localization of the radioactivity in PET images was suggestive of the right common carotid artery (arrowhead). PET-CT fused images confirmed that the thrombus was located about 1–2 cm proximal to the carotid bifurcation. An increase in radioactivity was also found around the surgical site.

FBP7 showed rapid and persistent uptake in the thrombus and fast clearance from non-target tissues. Figure 3A shows a coronal PET image from data collected 30–90 min p.i. The radioactivity was significantly higher in the thrombus compared with the background tissues (contralateral artery, brain, heart), as shown in Figure 3B; one-way ANOVA, P<0.0001. Time-activity curves obtained from the dynamic data showed a steady level of probe uptake at the thrombosed artery, whereas activity in other surrounding tissues decreased over time (Figure 3C). By 22 min p.i., thrombus had significantly higher activity than all the background tissues (Figure 3C; repeated measures ANOVA, P<0.0001). At 240–285 min

p.i., off-target background was almost undetectable, while a hyperintense signal was still present at the level of the thrombus (Figure 3D). Target-specific FBP7 accumulation combined with the reduction of background activity increased the difference in uptake between the thrombus and background tissues (Figure 3E; ANOVA, $P<0.0001$). This time-dependent reduction of the off-target activity contributed to an increase in thrombus-to-background ratio. In particular, for the 30–90 min p.i. image, there was a >5-fold difference between the thrombus and left carotid artery and this increased to >20-fold for the 240–285 min p.i. image; similarly there was >3-fold higher activity in the thrombus than in the heart at the early time point and this increased to >10-fold at the later time point (Figure 3F).

Ex vivo biodistribution studies confirmed the high uptake of FBP7 at the level of the thrombus (Figure 4A). At 120 min and 300 min p.i., the thrombus had the highest uptake (~0.4–0.5 %ID/g) after kidney and liver, although the uptake of the latter was very similar to the thrombus (~0.6 %ID/g). Very little activity remained in the animal at either 2 or 5 hours p.i. with the most retention observed in the kidneys, although this was quite low (1.74 ± 0.15% ID/g at 5 hours). Activity in the thrombus was similar at both time points, while the activity in most other organs decreased with time. This resulted in high thrombus-to-organ ratios at 2 hours p.i. that increased at the 5 hour time point. For example at 2 hours p.i. the thrombus had ≥5-fold higher activity than the contralateral vessel, heart, muscle, brain, or blood, and these ratios increased to ≥14-fold at 5 hours p.i. (Figure 4B). *Ex vivo* autoradiography confirmed the results obtained from PET and biodistribution. A hyperintense region was detected in the right carotid artery segment corresponding to the location where the artery was crushed, but not in contralateral vessel (Supplemental Figure IV). Ipsilateral-to-contralateral activity ratios obtained by autoradiography were 7.5 ± 3.1 and 13.3 ± 4.9 for 2 and 5 hours p.i., respectively. Histopathology revealed the presence of mural thrombi and fibrin deposition at the level of the right (ipsilateral) common carotid artery, but not contralaterally (Supplemental Figure V).

Thromboembolic stroke

Three animals were removed from the study according to our *a priori* exclusion criteria: two (one vehicle and one rtPA-treated) had premature death and autopsy revealed hemorrhage at the base of the skull, and in one rat that received rtPA the clot was not lysed. Biodistribution analysis showed no effect of rtPA treatment on background signal (not shown).

After FBP7 injection, an intracranial hyperintense region was clearly visible at the base of the brain in all the stroke rats. Figures 5A and 5B show orthogonal PET-CT images that bisect the intracranial clot. A hot spot was apparent in the ICA close to the origin of the right MCA, but not on the contralateral side. The presence and location of the thrombus were confirmed by postmortem visual examination of the circle of Willis (Figure 5C–D). PET images also showed hot spots at the surgical site as well as along the extracranial segments of the ICA, in particular before it enters the skull (Figure 5B), probably corresponding to the terminal portion of the 25-mm long embolus and the arterial denudation caused by the catheter insertion.[21] PET findings were congruent with the visual inspection of the circle of Willis as well as autoradiography, which revealed high activity along the ICA and MCA (Figure 5D–E). Histopathology confirmed the presence of an occlusive embolus in the right

(ipsilateral) MCA of rats subjected to embolic stroke and an immunopositive signal in the lumen of the vessel consistent with fibrin deposition (Supplemental Figure VI).

The initial hyperintense signal that was detected around the extracranial ICA in all the stroke animals (Figure 6A–B) was completely abolished after rtPA treatment (Figure 6C), whereas vehicle-treated animals continued to display high radioactivity (Figure 6D). Time-activity curves at the level of the extracranial thrombus revealed stable radioactivity in vehicle-injected rats and time-dependent reduction in rats treated with rtPA (Figure 6E; repeated measures ANOVA, $P<0.001$). Radioactivity ratios between ipsilateral and contralateral extracranial ICA showed comparable values in both experimental groups before vehicle or rtPA administration (Figure 6F). However, while ipsilateral-to-contralateral ratio increased over time in vehicle-injected animals, consistent with a stable signal enhanced by background attenuation, it decreased in rtPA-treated rats (Figure 6F; repeated measures ANOVA, $P<0.001$).

Post-thrombolytic reduction of the PET signal was also detected at the intracranial ICA-MCA level (Figure 7A–B). Baseline imaging showed no difference in the ratio of ipsilateral to contralateral ICA-MCA activity between groups (vehicle, 1.28±0.40, n=6; rtPA, 1.47±0.21, n=7; Student's t-test, $P>0.05$). After treatment, the ratio of ipsilateral to contralateral ICA-MCA activity was high in vehicle-treated rats (2.66±0.70), but significantly lower in animals treated with rtPA (1.08±0.11), as shown in Figure 7E (Student's t-test, $P<0.001$). Visual inspection of the circle of Willis (Figure 7C) and autoradiography (Figure 7D) confirmed clot dissolution and subsequent low activity in the intracranial ICA-MCA region after rtPA treatment. Autoradiography of rtPA-treated animals showed low activity at the level of the ipsilateral ICA-MCA, resulting in ipsilateral to contralateral ratio close to 1, while this ratio was over 5 for animals that received vehicle (Figure 7F).

Discussion

This study shows that the novel fibrin-binding probe FBP7 detects thrombosis and thrombolysis using PET-CT imaging. FBP7 showed high *in vitro* stability and nanomolar affinity to the fibrin surrogate DD(E), and this was not affected by the presence of heparin. We first demonstrated that FBP7 imaging is feasible to detect a hyperacute, non-occlusive thrombus formed in the common carotid artery following crush injury. The high probe uptake at the thrombus level (~0.5 %ID/g) provided excellent target-to-background contrast, which increased over time as activity cleared from background tissues and organs. We then assessed whether FBP7 could detect an aged, occlusive clot using a rat model of embolic stroke. After the injection of the probe, a hyperintense PET signal was detectable at the level of the ipsilateral MCA-ICA, but not contralaterally. Finally, we tested whether FBP7 was able to image and quantify *in vivo* clot lysis after thrombolytic treatment. Rats treated with rtPA showed reduced activity at the MCA-ICA segment, while a persistent high activity was detected in vehicle-injected animals. Overall, our findings show the efficacy of FBP7 as a new PET probe for molecular imaging of *in vivo* thrombosis and thrombolysis.

Thrombosis is a common feature of many major cardiovascular diseases and the early detection of thrombus formation is critical for both diagnosis and intervention. Different methods to image thrombosis are used clinically, depending on the vascular territory and the institutional resources. Some of these imaging techniques (e.g., ultrasound, TEE, CT, MR imaging) are quite efficacious and have been accepted as the gold standard in particular thrombus localizations.[10] However, since the sensitivity and specificity of these techniques show considerable degrees of variation depending on the site of thrombus, a combined imaging protocol that includes multiple techniques as a part of etiologic work-up is required in most patients.[4–7] One way to overcome this time consuming and expensive diagnostic approach is to shift the vasculature-specific focus of imaging to a pathology-specific focus (i.e., thrombus imaging). Accordingly, targeted probes for molecular imaging are emerging as powerful tools in cardiovascular medicine for the detection of thrombus with high sensitivity and specificity.[22] Since fibrin is the one of the main components of the thrombus, fibrin-targeted probes offer a great opportunity for thrombus imaging. In particular, fibrin-based MR probes have been extensively used in the past decade to detect thrombosis in both animal models and human trials.[11] However, one of the main limitations of molecular MRI is its low sensitivity which makes it challenging to detect low levels of target proteins. PET imaging has instead several advantages that make it suitable for cardiovascular applications, chief among them the high sensitivity and the ability to perform accurate quantification.[23] One of the main shortcomings is however the low spatial resolution, which has been partially overcome with the development of multimodal systems such as PET-CT or PET-MR. Indeed, dual imaging modalities are becoming widely used in cardiology, providing anatomical and physiological information for both diagnosis and follow-up studies.[24] On these bases, the availability of a PET probe with high sensitivity and specificity such as FBP7 can be valuable for both preclinical and clinical studies, especially if combined with a high spatial resolution system to localize the radiotracer concentration and to provide additional information (e.g., tissue perfusion, anatomical alterations).

In the present work, we showed that FBP7 can detect both freshly-formed (crush model) and aged thrombi (stroke model), congruent with previous findings using fibrin-targeted MR imaging probes.[21, 25–27] The probe FBP7 rapidly accumulates at the level of the thrombus, the third tissue with highest uptake after liver and kidneys, allowing a facile localization of the clot even in a wide field of view (see Supplemental Video I). This feature can be particularly useful for source thrombus detection in recurrent events, for example after recurrent ischemic stroke. The definition of stroke etiology is important to select the best treatment. After cardioembolic stroke, for example, anticoagulants have been shown to be more efficacious than aspirin to prevent recurrent episodes, while the same effect was not found in patients with stroke of non-cardioembolic origin.[28, 29] However, in 30–40% of ischemic stroke cases the etiology remains unknown and these strokes are classified as cryptogenic,[30] limiting the design of an appropriate therapy for the prevention of secondary stroke. The combination of highly sensitive imaging modalities and specific targeted-probes such as FBP7 can provide a new diagnostic approach to evaluate the source thrombus after embolism. The present study also suggests that FBP7 is useful as a monitoring tool. In rats with embolic stroke, FBP7 enabled visualization of rtPA-induced thrombolysis. FBP7

imaging could be used to monitor treatment efficacy either after an acute intervention or after a regimen of anticoagulants.

FBP7 shows a superior metabolic stability compared to our previous fibrin-targeted PET probes.[15–17] We previously used the DOTA chelator to envelop the copper-64 ion.[15, 16] However, the DOTA based probes showed some dissociation of the metal ion from the probe which resulted in increased liver uptake and binding of the copper-64 to plasma proteins. This latter effect resulted in persistent blood background which limited the thrombus-to-background ratio.[16] To reduce the issue of copper dissociation, we replaced DOTA with the CB-TE2A chelator, which is expected to form more inert complexes with copper.[31, 32] This chelate modification in FBP7 drastically reduced the dissociation, resulting in more than 70% of intact probe in the blood even after four hours p.i. Due to the improved stability, very little Cu-64 is released to bind to plasma proteins, while the intact small probe FBP7 is rapidly eliminated by the kidneys and this results in rapid systemic clearance of the activity. The affinity for fibrin is sufficient such that activity in the thrombus persists over at least 5 hours resulting in high target:background ratios that increase with time. The fast systemic clearance is a major pharmacokinetic advantage for the small FBP7 probe especially in comparison with other thrombus-targeted imaging approaches (such as antibodies which exhibit long half-lives in blood causing low target-to-background ratios).[33, 34]

Compared with other commonly used PET radionuclides (e.g., fluorine-18), copper-64 has a longer half-life (110 min vs. 12.7 hours, respectively). This means that the probe can be synthesized in advance and be ready to use when needed or even produced remotely and then shipped on demand. The latter feature is useful for institutions that are geographically isolated from a cyclotron. While a longer half-life can raise radiation exposure concerns, FBP7 showed rapid whole body elimination with very little activity retained in the kidneys and liver at the 5 hours time point. On the other hand, due to its chemical properties, fast clearance, and the rapid target-specific accumulation, our fibrin-binding peptide could be readily labeled with radionuclides with shorter half-lives (e.g., fluorine-18, gallium-68), although we expect blood clearance to be slower in humans compared to rats because of lower cardiac output.

The peptide used in FBP7 is a derivative of that used in the MR probe EP-2104R. EP-2104R was evaluated in small Phase II trial for the detection of thrombus in the deep veins, the lungs, cardiac chambers, ascending aorta, and carotid arteries.[35] While EP-2104R showed promise in thrombus detection, clots were more conspicuous at 2 hours or later post probe injection. For MR imaging, where a baseline image is required, this resulted in two imaging sessions and is not ideal for patient workflow or for comparing the pre- and post-probe images. The PET technique does not suffer this limitation as a baseline scan is not required. There is also a much lower safety risk of the PET probe due to the much lower mass dose compared to MR imaging, although this is offset by the radiation exposure with PET.

In our study we found about 2- to 3-fold lower thrombus:background ratios for the intracranial clots compared to the extracranial thrombi when measured by PET imaging. However *ex vivo* autoradiography showed comparable ipsi:contra ratios between the intra-

and extracranial thrombi. Histology also revealed that the intracranial clots were fibrin rich. This discrepancy between the PET imaging and autoradiography is due to a partial volume effect related to the vessel size (internal diameter in adult rats are >600 μm for extracranial ICA, ~200–360 μm for intracranial ICA and MCA),[36] where the thrombus is smaller than the resolution of the micro-PET camera used for the present study (~1.2 mm). For smaller thrombi, this partial volume loss is more pronounced and will ultimately limit the size of thrombus that can be detected. On the other hand, the very high target:background achieved with FBP7 already demonstrates that we can still detect pathology well below the resolution limit of the PET camera (e.g., the MCA thrombus occupies at most $1/10^{th}$ of a PET voxel). Combining PET with CT also provided valuable anatomical context that enables confident diagnosis of small thrombi.

Study limitations

There are some limitations in the present study, including the small sample size and the animal models which do not entirely mimic the clinical setting. We did not perform any specific experiment to assess whether FBP7 is able to visualize clots older than 24 hours, but previous works have shown that fibrin-targeted probes can detect aged and organized thrombi.[37] Thrombus aging is a dynamic process and time-dependent changes in thrombus composition (e.g., fibrin content) affect clot stability and thus thrombolysis.[38] Future studies are needed to assess the time window of efficacy for FBP7, as well as its potential to discriminate between different stages of thrombus formation based on fibrin content.

Conclusion

In this study, we demonstrated the feasibility of PET imaging of thrombosis and thrombolysis using a new fibrin-binding probe. FBP7 imaging detected both non-occlusive (mural) and occlusive thrombi; furthermore, FBP7 enabled both visualization and quantification of *in vivo* thrombolysis following rtPA treatment. Indeed, FBP7 represents a very promising candidate for translation in clinical testing.

Supplementary Material

Refer to Web version on PubMed Central for supplementary material.

Acknowledgments

Prof. Carolyn Anderson of the University of Pittsburgh Medical Center is gratefully acknowledged for a gift of the cross-bridged chelator CB-TE2A used in this study.

Sources of Funding

This work was supported by HL109448 (to P. C.) from the National Heart, Lung, and Blood Institute, and the micro-PET/SPECT/CT system was funded by RR029495 (to A.-L. B.) from the National Center for Research Resources. This research was carried out in whole at the Athinoula A. Martinos Center for Biomedical Imaging at the Massachusetts General Hospital, using resources provided by the Center for Functional Neuroimaging Technologies, P41RR14075, a P41 Regional Resource supported by the Biomedical Technology Program of the National Center for Research Resources, NIH.

References

1. Go AS, Mozaffarian D, Roger VL, Benjamin EJ, Berry JD, Blaha MJ, Dai S, Ford ES, Fox CS, Franco S, Fullerton HJ, Gillespie C, Hailpern SM, Heit JA, Howard VJ, Huffman MD, Judd SE, Kissela BM, Kittner SJ, Lackland DT, Lichtman JH, Lisabeth LD, Mackey RH, Magid DJ, Marcus GM, Marelli A, Matchar DB, McGuire DK, Mohler ER 3rd, Moy CS, Mussolino ME, Neumar RW, Nichol G, Pandey DK, Paynter NP, Reeves MJ, Sorlie PD, Stein J, Towfighi A, Turan TN, Virani SS, Wong ND, Woo D, Turner MB. American Heart Association Statistics C, Stroke Statistics S. Heart disease and stroke statistics--2014 update: a report from the American Heart Association. Circulation. 2014; 129:e28–e292. [PubMed: 24352519]
2. Hillen T, Coshall C, Tilling K, Rudd AG, McGovern R, Wolfe CD. Cause of stroke recurrence is multifactorial: patterns, risk factors, and outcomes of stroke recurrence in the South London Stroke Register. Stroke. 2003; 34:1457–63. [PubMed: 12750544]
3. Sipola P, Hedman M, Onatsu J, Turpeinen A, Halinen M, Jakala P, Vanninen R. Computed tomography and echocardiography together reveal more high-risk findings than echocardiography alone in the diagnostics of stroke etiology. Cerebrovasc Dis. 2013; 35:521–30. [PubMed: 23817231]
4. Markel A, Weich Y, Gaitini D. Doppler ultrasound in the diagnosis of venous thrombosis. Angiology. 1995; 46:65–73. [PubMed: 7818159]
5. Kronzon I, Tunick PA. Aortic atherosclerotic disease and stroke. Circulation. 2006; 114:63–75. [PubMed: 16818829]
6. Srichai MB, Junor C, Rodriguez LL, Stillman AE, Grimm RA, Lieber ML, Weaver JA, Smedira NG, White RD. Clinical, imaging, and pathological characteristics of left ventricular thrombus: a comparison of contrast-enhanced magnetic resonance imaging, transthoracic echocardiography, and transesophageal echocardiography with surgical or pathological validation. Am Heart J. 2006; 152:75–84. [PubMed: 16824834]
7. Litmanovich D, Bankier AA, Cantin L, Raptopoulos V, Boiselle PM. CT and MRI in diseases of the aorta. AJR Am J Roentgenol. 2009; 193:928–40. [PubMed: 19770313]
8. Beyer T, Townsend DW, Czernin J, Freudenberg LS. The future of hybrid imaging-part 2: PET/CT. Insights Imaging. 2011; 2:225–34. [PubMed: 23099865]
9. Beyer T, Freudenberg LS, Czernin J, Townsend DW. The future of hybrid imaging-part 3: PET/MR, small-animal imaging and beyond. Insights Imaging. 2011; 2:235–246. [PubMed: 22347950]
10. Lindner JR. Molecular imaging of thrombus: technology in evolution. Circulation. 2012; 125:3057–9. [PubMed: 22647974]
11. Ciesienski KL, Caravan P. Molecular MRI of Thrombosis. Curr Cardiovasc Imaging Rep. 2010; 4:77–84. [PubMed: 21253438]
12. Kolodziej AF, Nair SA, Graham P, McMurry TJ, Ladner RC, Wescott C, Sexton DJ, Caravan P. Fibrin specific peptides derived by phage display: characterization of peptides and conjugates for imaging. Bioconjug Chem. 2012; 23:548–56. [PubMed: 22263840]
13. Overoye-Chan K, Koerner S, Looby RJ, Kolodziej AF, Zech SG, Deng Q, Chasse JM, McMurry TJ, Caravan P. EP-2104R: a fibrin-specific gadolinium-Based MRI contrast agent for detection of thrombus. J Am Chem Soc. 2008; 130:6025–39. [PubMed: 18393503]
14. Botnar RM, Perez AS, Witte S, Wiethoff AJ, Laredo J, Hamilton J, Quist W, Parsons EC Jr, Vaidya A, Kolodziej A, Barrett JA, Graham PB, Weisskoff RM, Manning WJ, Johnstone MT. In vivo molecular imaging of acute and subacute thrombosis using a fibrin-binding magnetic resonance imaging contrast agent. Circulation. 2004; 109:2023–9. [PubMed: 15066940]
15. Uppal R, Catana C, Ay I, Benner T, Sorensen AG, Caravan P. Bimodal thrombus imaging: simultaneous PET/MR imaging with a fibrin-targeted dual PET/MR probe--feasibility study in rat model. Radiology. 2011; 258:812–20. [PubMed: 21177389]
16. Ciesienski KL, Yang Y, Ay I, Chonde DB, Loving GS, Rietz TA, Catana C, Caravan P. Fibrin-targeted PET probes for the detection of thrombi. Mol Pharmaceutics. 2013; 10:1100–10.
17. Boros E, Rybak-Akimova E, Holland JP, Rietz T, Rotile N, Blasi F, Day H, Latifi R, Caravan P. Pycup-A bifunctional, cage-like ligand for (64)Cu radiolabeling. Mol Pharmaceutics. 2014; 11:617–29.

18. Zhang RL, Chopp M, Zhang ZG, Jiang Q, Ewing JR. A rat model of focal embolic cerebral ischemia. Brain Res. 1997; 766:83–92. [PubMed: 9359590]
19. Zhang ZG, Zhang L, Ding G, Jiang Q, Zhang RL, Zhang X, Gan WB, Chopp M. A model of mini-embolic stroke offers measurements of the neurovascular unit response in the living mouse. Stroke. 2005; 36:2701–4. [PubMed: 16269633]
20. Loening AM, Gambhir SS. AMIDE: a free software tool for multimodality medical image analysis. Mol Imaging. 2003; 2:131–7. [PubMed: 14649056]
21. Uppal R, Ay I, Dai G, Kim YR, Sorensen AG, Caravan P. Molecular MRI of intracranial thrombus in a rat ischemic stroke model. Stroke. 2010; 41:1271–7. [PubMed: 20395615]
22. Buxton DB, Antman M, Danthi N, Dilsizian V, Fayad ZA, Garcia MJ, Jaff MR, Klimas M, Libby P, Nahrendorf M, Sinusas AJ, Wickline SA, Wu JC, Bonow RO, Weissleder R. Report of the National Heart, Lung, and Blood Institute working group on the translation of cardiovascular molecular imaging. Circulation. 2011; 123:2157–63. [PubMed: 21576680]
23. Dobrucki LW, Sinusas AJ. PET and SPECT in cardiovascular molecular imaging. Nat Rev Cardiol. 2010; 7:38–47. [PubMed: 19935740]
24. Fayad ZA, Mani V, Woodward M, Kallend D, Abt M, Burgess T, Fuster V, Ballantyne CM, Stein EA, Tardif JC, Rudd JH, Farkouh ME, Tawakol A, dal PI. Safety and efficacy of dalcetrapib on atherosclerotic disease using novel non-invasive multimodality imaging (dal-PLAQUE): a randomised clinical trial. Lancet. 2011; 378:1547–59. [PubMed: 21908036]
25. Sirol M, Aguinaldo JG, Graham PB, Weisskoff R, Lauffer R, Mizsei G, Chereshnev I, Fallon JT, Reis E, Fuster V, Toussaint JF, Fayad ZA. Fibrin-targeted contrast agent for improvement of in vivo acute thrombus detection with magnetic resonance imaging. Atherosclerosis. 2005; 182:79–85. [PubMed: 16115477]
26. Spuentrup E, Fausten B, Kinzel S, Wiethoff AJ, Botnar RM, Graham PB, Haller S, Katoh M, Parsons EC Jr, Manning WJ, Busch T, Gunther RW, Buecker A. Molecular magnetic resonance imaging of atrial clots in a swine model. Circulation. 2005; 112:396–9. [PubMed: 16009790]
27. Spuentrup E, Buecker A, Katoh M, Wiethoff AJ, Parsons EC Jr, Botnar RM, Weisskoff RM, Graham PB, Manning WJ, Gunther RW. Molecular magnetic resonance imaging of coronary thrombosis and pulmonary emboli with a novel fibrin-targeted contrast agent. Circulation. 2005; 111:1377–82. [PubMed: 15738354]
28. Halperin JL, Hart RG, Kronmal RA, McBride R, Pearce LA, Sherman DG. Warfarin versus aspirin for prevention of thromboembolism in atrial fibrillation: Stroke Prevention in Atrial Fibrillation II Study. Lancet. 1994; 343:687–91. [PubMed: 7907677]
29. Mohr JP, Thompson JL, Lazar RM, Levin B, Sacco RL, Furie KL, Kistler JP, Albers GW, Pettigrew LC, Adams HP Jr, Jackson CM, Pullicino P. A comparison of warfarin and aspirin for the prevention of recurrent ischemic stroke. N Engl J Med. 2001; 345:1444–51. [PubMed: 11794192]
30. Guercini F, Acciarresi M, Agnelli G, Paciaroni M. Cryptogenic stroke: time to determine aetiology. J Thromb Haemost. 2008; 6:549–54. [PubMed: 18208534]
31. Garrison JC, Rold TL, Sieckman GL, Figueroa SD, Volkert WA, Jurisson SS, Hoffman TJ. In vivo evaluation and small-animal PET/CT of a prostate cancer mouse model using 64Cu bombesin analogs: side-by-side comparison of the CB-TE2A and DOTA chelation systems. J Nucl Med. 2007; 48:1327–37. [PubMed: 17631556]
32. Boswell CA, Sun X, Niu W, Weisman GR, Wong EH, Rheingold AL, Anderson CJ. Comparative in vivo stability of copper-64-labeled cross-bridged and conventional tetraazamacrocyclic complexes. J Med Chem. 2004; 47:1465–74. [PubMed: 14998334]
33. Cerqueira MD, Stratton JR, Vracko R, Schaible TF, Ritchie JL. Noninvasive arterial thrombus imaging with 99mTc monoclonal antifibrin antibody. Circulation. 1992; 85:298–304. [PubMed: 1728460]
34. Olafsen T, Wu A. Antibody vectors for imaging. Semin Nucl Med. 2010; 40:167–181. [PubMed: 20350626]
35. Vymazal J, Spuentrup E, Cardenas-Molina G, Wiethoff AJ, Hartmann MG, Caravan P, Parsons EC Jr. Thrombus imaging with fibrin-specific gadolinium-based MR contrast agent EP-2104R: results of a phase II clinical study of feasibility. Invest Radiol. 2009; 44:697–704. [PubMed: 19809344]

36. Nordborg C, Fredriksson K, Johansson BB. The morphometry of consecutive segments in cerebral arteries of normotensive and spontaneously hypertensive rats. Stroke. 1985; 16:313–20. [PubMed: 3975970]

37. Sirol M, Fuster V, Badimon JJ, Fallon JT, Moreno PR, Toussaint JF, Fayad ZA. Chronic thrombus detection with in vivo magnetic resonance imaging and a fibrin-targeted contrast agent. Circulation. 2005; 112:1594–600. [PubMed: 16145001]

38. Brommer EJ, van Bockel JH. Composition and susceptibility to thrombolysis of human arterial thrombi and the influence of their age. Blood Coagul Fibrinolysis. 1992; 3:717–25. [PubMed: 1489893]

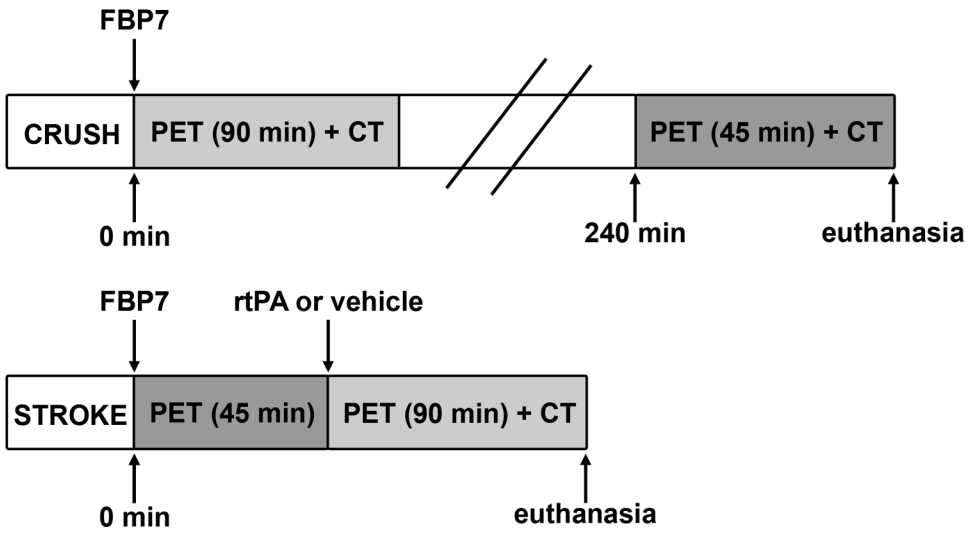

Figure 1.

Timeline of the carotid crush injury (CRUSH) and embolic stroke (STROKE) experiments. All rats were injected with the PET probe FBP7 immediately after the surgery. In CRUSH experiments, rats were imaged immediately or 240 min after the injury. In STROKE experiments, animals were imaged for 45 min, injected with rtPA or vehicle, and imaged for additional 90 min.

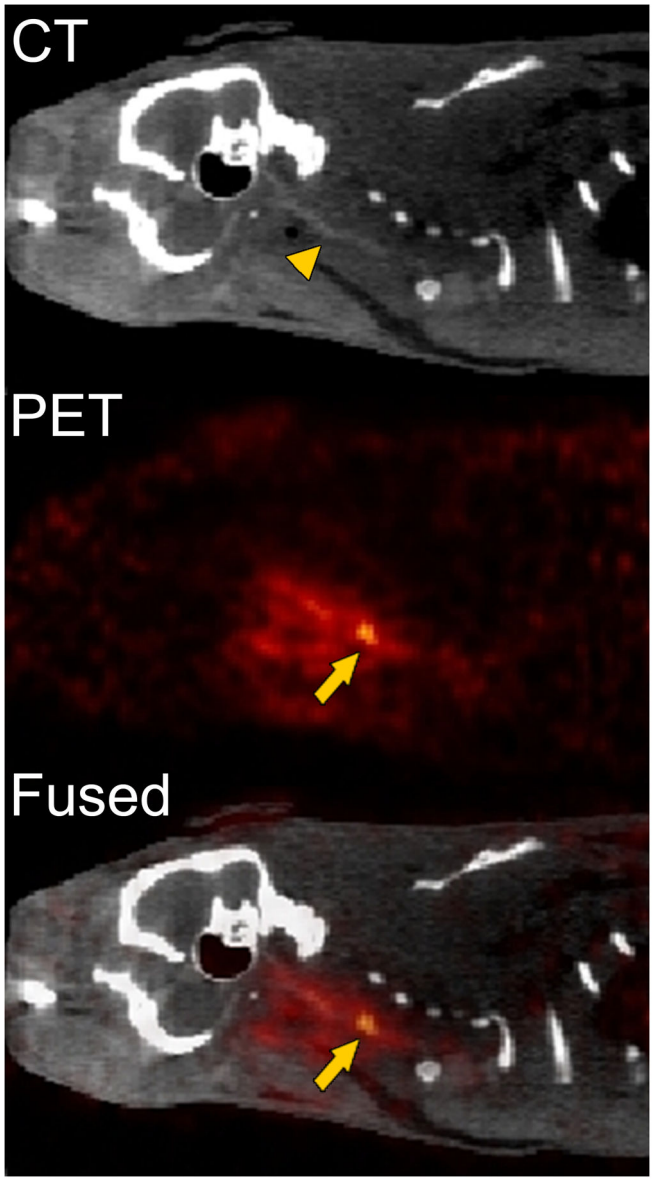

Figure 2.

Representative CT, PET, and fused PET-CT sagittal images reconstructed from data 240–285 min after the injection of FBP7 obtained from an animal that had carotid crush injury. FBP7 imaging reveals the thrombus localization at the level of the common carotid artery. Arrows indicate the crush injury site; arrowhead indicates the common carotid artery.

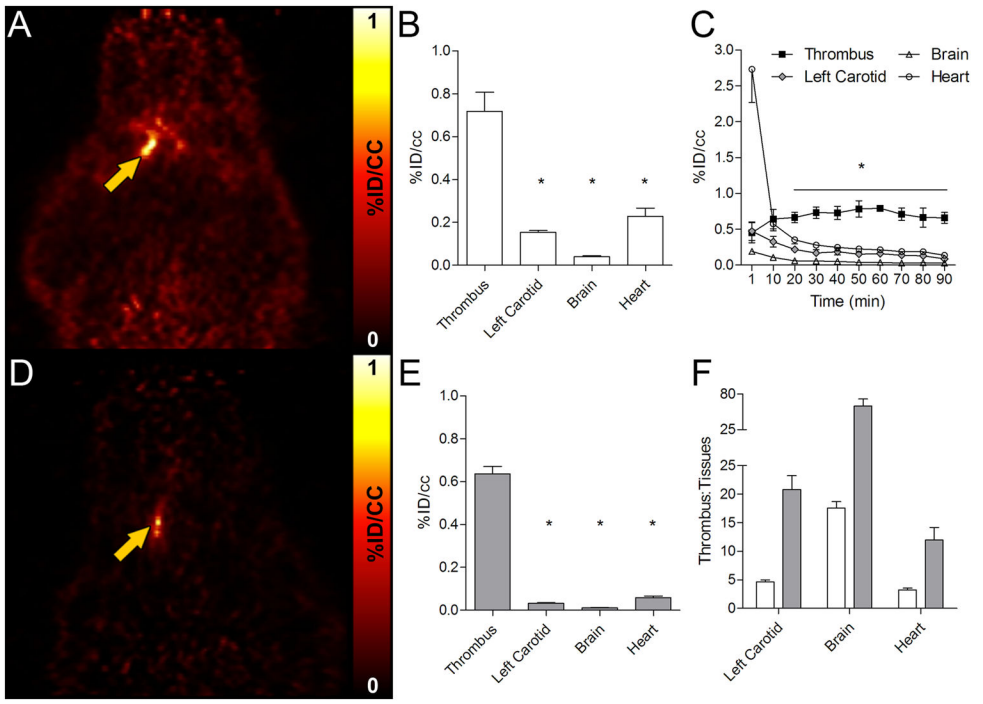

Figure 3.

Results of 30–90 min (A, B, C, F) and 240–285 min (D, E, F) PET scans. After the carotid crush injury, target-to-background increases over time after FBP7 injection. PET images from representative animals obtained at 30–90 min (A) and 240–285 min (D) post-injection showed persistent thrombus signal and a decrease in the background activity over time. PET activity analysis demonstrated that the artery containing the thrombus had significantly more activity compared to background tissues at 30–90 min post-injection (B) and this difference was pronounced at 240–285 min post-injection (E). Time-activity curves of the thrombus and background tissues (C). PET activity ratios between the thrombus and background tissues over time (F. White bars: 30–90 min post-injection; gray bars: 240–285 min post-injection). Error bars represent S.E.M. *P<0.0001.

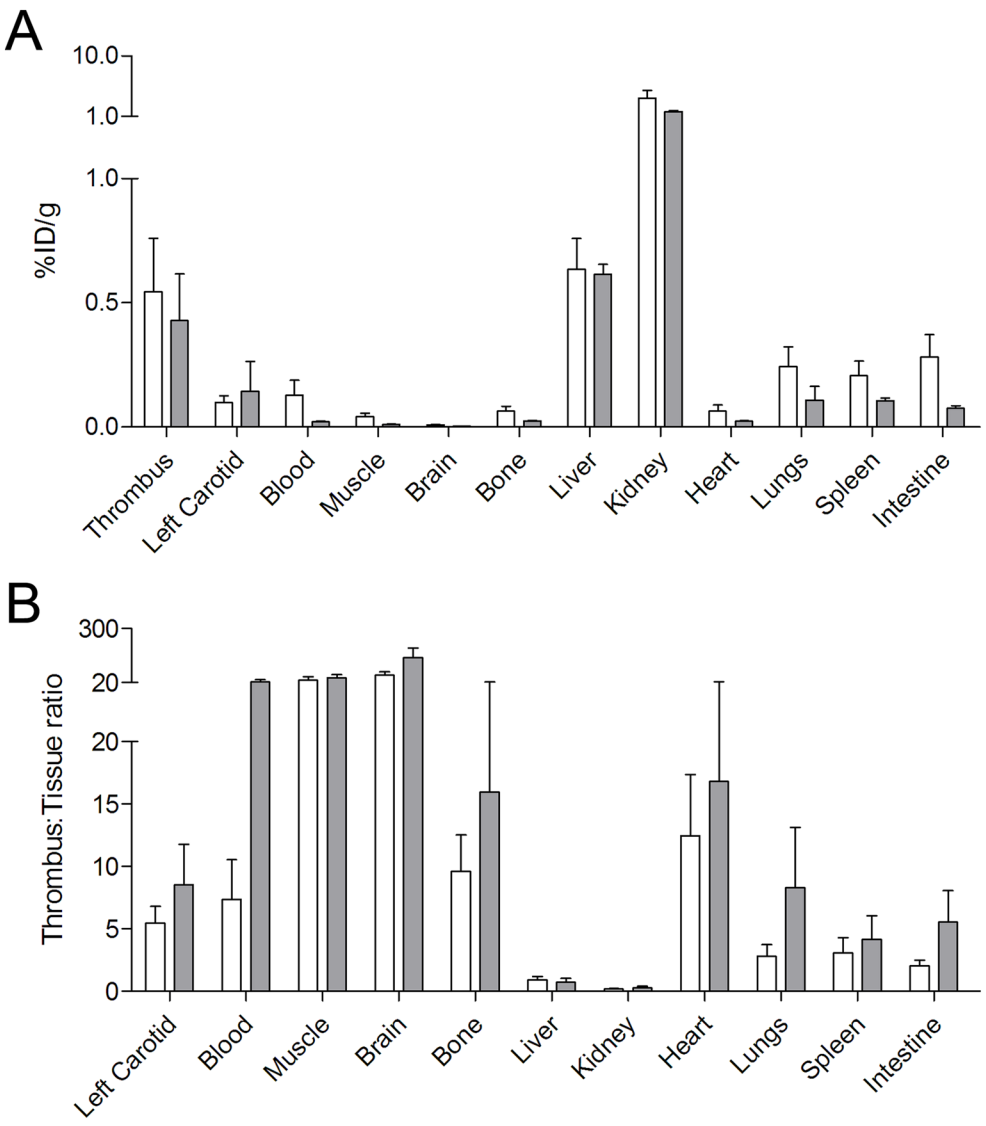

Figure 4.

Biodistribution studies confirmed high thrombus uptake of FBP7. White bars: 30–90 min post-injection; gray bars: 240–285 min post-injection. Error bars represent S.E.M.

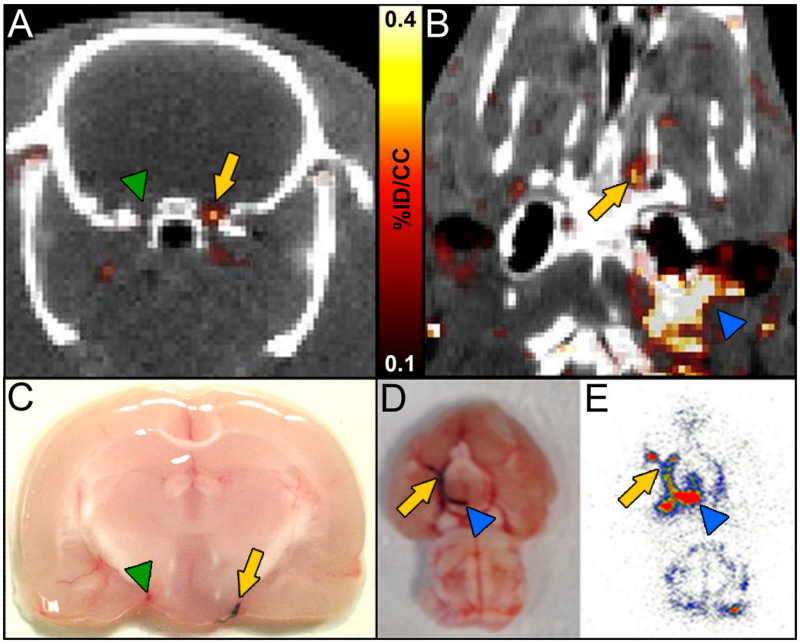

Figure 5.

PET-CT images showed that FBP7 detects occlusive thrombus in both intracranial (AB) and extracranial (B) arteries. A: arrow = ICA/MCA with thrombus; green arrowhead = contralateral ICA/MCA. B: arrow = intracranial ICA/MCA; blue arrowhead = extracranial ICA. Presence of thrombus was verified in postmortem brains from animals injected with Evans blue-labeled clot (C–D; arrow in C = ICA/MCA with thrombus; green arrowhead in C = contralateral ICA/MCA; arrow in D = intracranial ICA/MCA; blue arrowhead in D = extracranial ICA). Autoradiography replicated findings of PET-CT (E; arrow = intracranial ICA/MCA; blue arrowhead = extracranial ICA).

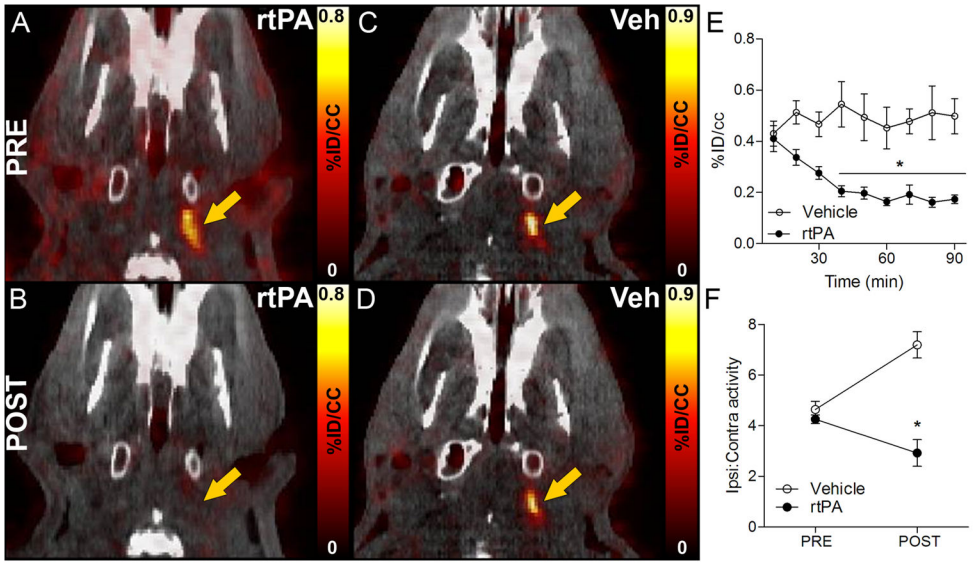

Figure 6.

FBP7 enabled in vivo visualization of thrombolysis in extracranial ICA. A–D: Representative pre and post PET-CT images at the level of the extracranial ICA (arrow) from rtPA- and vehicle-treated animals. E: activity at the level of the extracranial ICA showed time-dependent reduction of signal after rtPA treatment (black circles) and steady signal in vehicle-injected rats (white circles). F: Ipsilateral-to-contralateral activity ratios before and after rtPA (black circles) and vehicle (white circles) administration. Error bars represent S.E.M. *P<0.05.

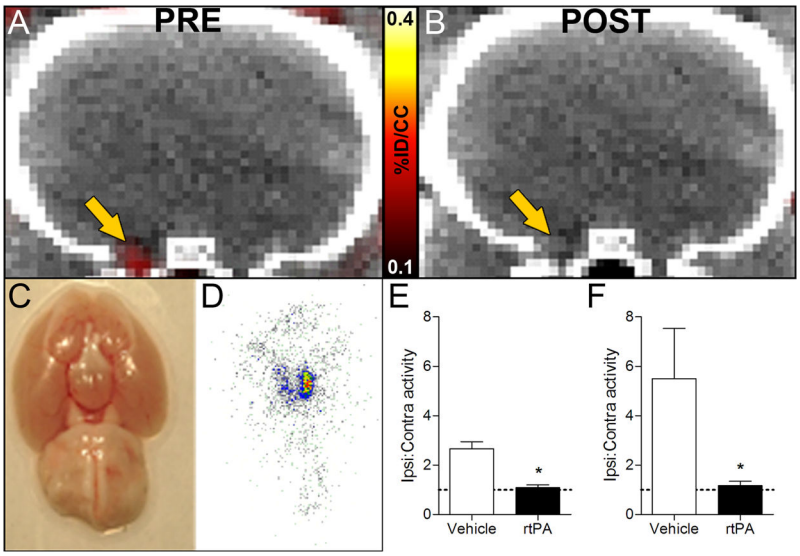

Figure 7.

FBP7 detected intracranial thrombolysis. A–B: Representative pre and post PET-CT images at the level of the intracranial ICA/MCA (arrow). Absence of thrombus was verified in postmortem brains (C) and autoradiography (D). Results of ipsilateral-to-contralateral activity ratios in rtPA- (black bars) and vehicle-treated (white bars) animals obtained from PET (E) and autoradiography (F) experiments. Dashed lines show ratio=1. Error bars represent S.E.M. *P<0.05.